Revealing deformation microstructures

A variety of features broadly classed as deformation microstructure elements are created during the plastic deformation of polycrystalline metals. While virtually all elements of deformation microstructure are composed of dislocations, describing the creation and evolution of larger-scale elements in terms of interactions between individual dislocations is a goal that has not yet been achieved. A hierarchical approach is thus favored in which structure creation and evolution are described at a range of length scales, from the nanometer to millimeter scale.

John A. Wert*, Xiaoxu Huang, Grethe Winther, Wolfgang Pantleon, and Henning F. Poulsen

Center for Fundamental Research: Metal Structures in Four Dimensions, Materials Research Department, Risø National Laboratory, Technical University of Denmark, 4000 Roskilde, Denmark

**E-mail: john.wert@risoe.dk*

The beautiful macroscopic patterns visible on Damascus steel[1] and the legendary sharpness and strength of swords made from this steel remind us of the link between the internal structure of metals and alloys and their engineering utility. The application of optical microscopy methods to study metallic materials[2] permitted a more detailed inspection of metal structures and was the first milestone in the development of a broad array of modern imaging methods. Transmission electron microscopy (TEM)[3] is perhaps the most widely applied imaging method today, but advanced optical[4] and X-ray imaging methods[5] are in a phase of rapid development. Diffraction methods have also played a key role in the study of metal structures, identifying the ordered atomic arrangement characteristic of crystalline metals[6] and enabling measurement of crystal orientations[7]. X-ray and electron diffraction have played key roles in the study of deformation structures in metals, particularly on the topic of texture development during thermomechanical processing[8]. Diffraction-based techniques for localized crystal orientation measurements, such as electron backscatter diffraction (EBSD)[9,10] and three-dimensional X-ray diffraction (3DXRD) methods using synchrotron X-ray sources[11], are of central importance today for characterizing fine-scale microstructural features.

These techniques, and the studies they enable, have engendered a broad materials research field that the pioneering developers of the techniques could scarcely have imagined. It would surely not surprise these experienced researchers, though, that many questions about metal structures remain incompletely answered despite the sophistication of modern measurement and modeling capabilities. Here we survey current understanding of metal microstructures created by plastic deformation processes.

ISSN:1369 7021 © Elsevier Ltd 2007

The motion of a particular line defect (dislocation – discovered independently by Orowan[12], Polanyi[13] , and Taylor[14] in 1934) is the primary microscopic agent of plastic deformation in metals. Thus, the description of deformation microstructures in terms of dislocation arrangements seems obvious. However, the enormous proliferation of dislocations associated with even moderate macroscopic strains renders a universal description of deformation microstructures in terms of individual dislocations impractical. Instead, dislocation structures are associated with a length-scale hierarchy (Fig. 1). For metals with grain sizes in the conventional range (larger than ~1 μm), microstructural elements smaller than ~1 μm are described in terms of individual dislocations and their interactions. Larger-scale microstructural elements, comprising boundaries of dislocations drawn together by mutual interactions, form the next structural level. While it is possible to describe the dislocation content of such a boundary in terms of idealized dislocation arrangements, identifying the arrangement that actually exists in any given boundary is difficult in practice[15]. Finally, in materials with grain sizes significantly greater than 1 μm, a larger scale structure exists: a structure related to the subdivision of grains into orientation domains that reflect differences in the activity of various slip systems.

Fig. 1 also illustrates the influence of initial grain size on the ability of a metal to sustain the processes by which microstructural elements with different sizes are created. For grain sizes at the nanoscale (substantially less than 1 μm), the interactions that lead to the formation of larger structural elements are forestalled, and the primary interactions are between individual dislocations and pre-existing boundaries. While such interactions also occur when the grain size is larger, their relative importance is diminished because fewer dislocations encounter a pre-existing boundary during the course of their motion. Thus, a practical definition of nanoscale metallic materials could be based on whether the primary interactions that determine material properties are dislocation/pre-existing boundary, or dislocation/dislocation interactions.

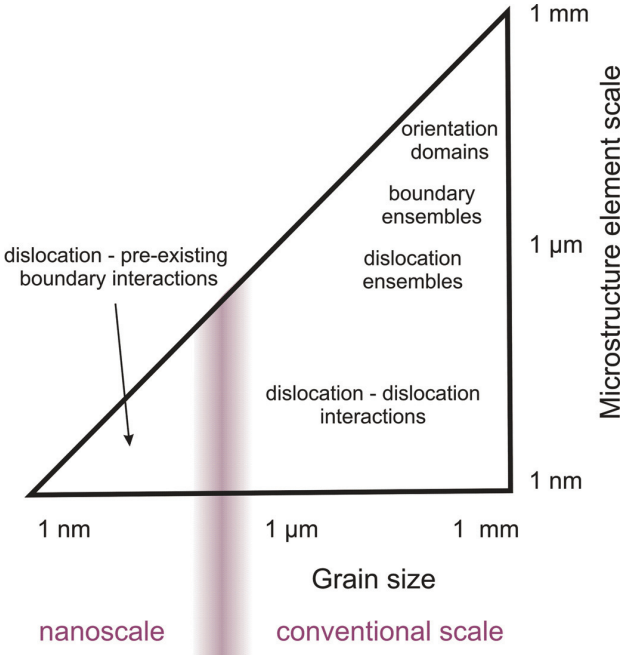

Fig. 1 Schematic of length scales associated with elements of deformation microstructure compared with the grain size. Only elements of deformation microstructure that form within grains are considered in this article. Features that would lie at the upper left corner of the figure, such as grain clusters and macroscopic deformation inhomogeneities, are beyond the scope of our considerations.

Although Fig. 1 portrays a static picture, elements of deformation microstructures evolve as functions of strain, in general shifting to smaller size scales with increasing strain. Thus, one can envision that the labels in Fig. 1 occupy a somewhat higher position on the vertical scale at the start of deformation and migrate downward to some degree as deformation proceeds. At sufficiently high strains, high-angle boundaries introduced during the course of deformation may become indistinguishable from pre-existing grain boundaries. In such cases, the spacing of all high-angle boundaries – irrespective of origin – substitutes for the grain size in Fig. 1 during subsequent deformation increments. The microstructures and stress–strain behavior of nanostructured metals created by high-strain deformation are described in the section on formation of nanostructured metals by plastic deformation. Fig. 1 also omits strain rate and temperature variables. While these parameters can profoundly influence deformation microstructures resulting from hot working processes, for example, they only modestly affect deformation microstructures produced during room-temperature deformation of metals with melting points exceeding 800 K or 900 K, the deformation conditions of primary interest in the present article.

Dislocation ensembles

In most metals, plastic deformation is caused by the lateral shift of crystalline lattice planes with respect to each other. The slip events are generated by glide motion of dislocations[16], which separate areas on glide planes that have slipped from areas that have not. In this manner, dislocations mark heterogeneities in plastic deformation and introduce elastic distortions in the crystalline lattice[17]. Dislocations are associated with both long-range elastic stresses and strains, and with rotations of the crystalline lattice. During the course of deformation, dislocations accumulate in crystals[18,19] as a result of entrapment by interactions with other dislocations or with microstructural features such as particles.

The interactions between dislocations are responsible for resistance to further deformation; thus, accumulation of dislocations causes work-hardening. The mutual interactions give rise to nonrandom dislocation arrangements: if dislocations are able to leave their glide plane[20,21], they gather in dislocation-rich walls (boundaries), leaving other regions depleted of dislocations. The emergence of such ordered dislocation

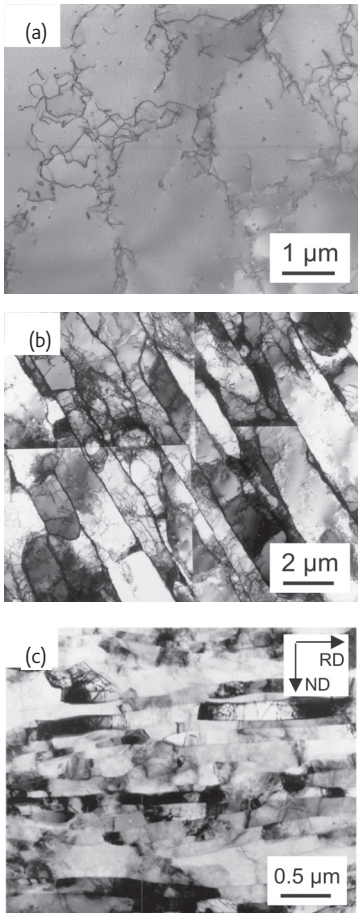

Fig. 2 TEM images of deformation microstructures. Dislocations appear black. Two distinct dislocation boundary types can be distinguished in (b) and (c) by their morphology. The curved boundaries (IDBs) originate from mutual trapping of dislocations whereas the planar dislocation boundaries (GNBs) result from differences in activated slip systems in the adjoining crystallites.

arrangements has been frequently observed by TEM, for instance, in Cu[22,23] or in Al[24] as in Fig. 2. From their different morphologies, different types of boundaries have been identified[25]: extended planar dislocation boundaries (termed geometrically necessary boundaries, GNBs) and loose curved cell walls (termed incidental dislocation boundaries, IDBs). The terms reflect their assumed origin: IDBs form by statistical mutual capture processes, while GNBs result from differences in activated slip systems on the adjoining crystallites.

Because thin foils less than a few micrometers thick are required for TEM investigations, the nature of the observed boundary structures has been debated[26]: are they representative of the structure during deformation, or are they artifacts from thinning? Attempts have been made to fix the dislocation structure by neutron irradiation[27] and no qualitative structural changes are observed between specimens irradiated before or after unloading[28]. However, such *post mortem* investigations (after deformation) cannot prove the existence of an ordered dislocation structure during deformation. Results from *in situ* investigations of structure formation during plastic deformation are similarly inconclusive because they can only be performed by TEM using thin foil specimens in which dislocations are affected by image forces caused by the free surfaces.

A novel X-ray diffraction technique[29,30] using high energy synchrotron X-ray radiation has been established at the Advanced Photon Source at Argonne National Laboratory. By reciprocal space mapping with high angular resolution of reflections from individual grains in a bulk specimen, structure formation *in situ* during tensile deformation of macroscopic specimens can be monitored. Depending on the material, different characteristics are observed (Fig. 3). For an Al-Mg alloy in which dislocation boundary formation is inhibited, the diffraction peak is a structureless cloud[31]. Whereas for Cu, which readily forms dislocation boundary structures, bright sharp peaks

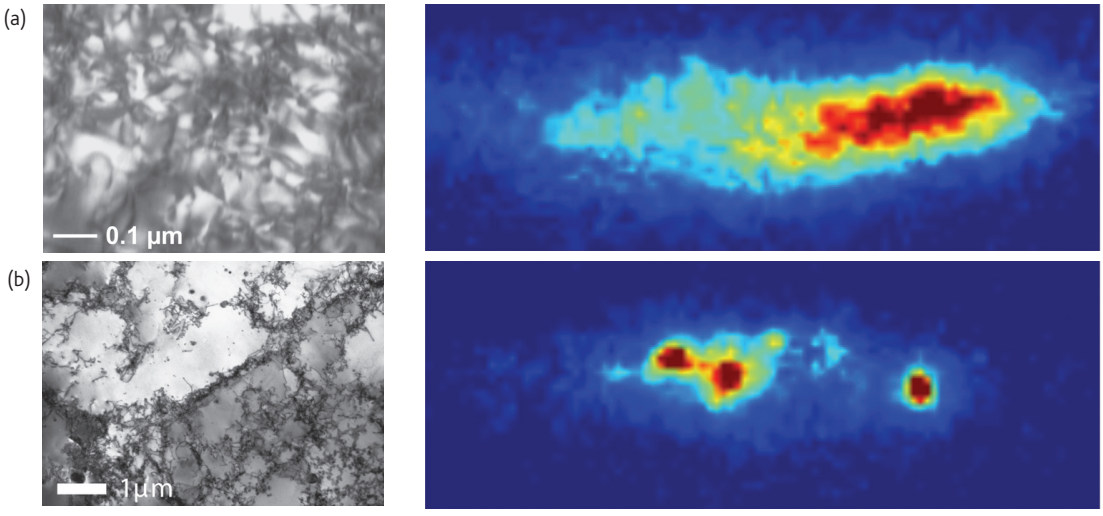

Fig. 3 Deformation structure after tensile deformation of (a) an Al–Mg alloy and (b) Cu, as resolved by TEM (left) and high angular resolution X-ray diffraction (right)[31]. The homogeneous dislocation distribution in the Al–Mg alloy causes a broadened X-ray reflection. The dislocation-free regions in the deformation structure of Cu give rise to the bright peaks superposed on a diffuse cloud stemming from the dislocation walls.

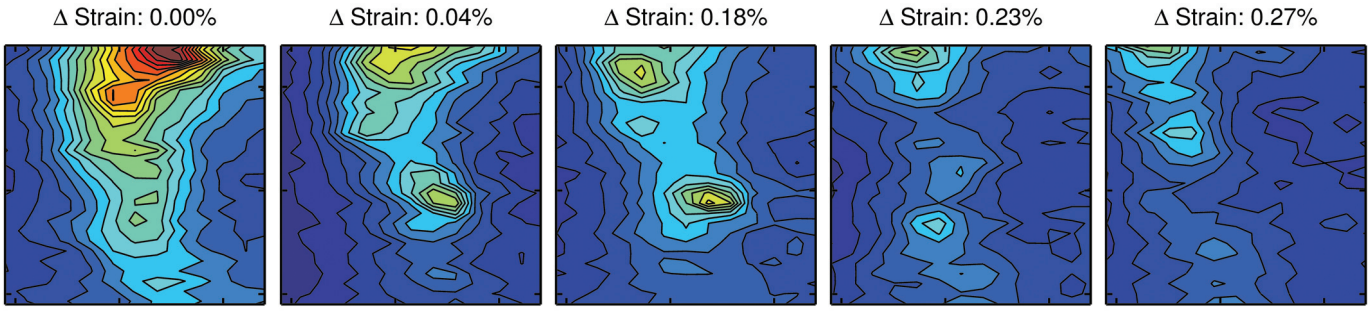

Fig. 4 Single peak in an X-ray reflection appearing and disappearing during the course of plastic deformation, indicating the intermittent dynamics of the dislocation-free regions during tensile deformation of Cu[29].

superimposed onto a structureless cloud are observed[29,30]. In the case of Cu, the diffuse cloud is thought to originate from the disordered dislocation arrangements in the boundaries, whereas the sharp peaks are identified as originating from nearly dislocation-free regions in the deformed specimen. During *in situ* tensile experiments, sharp diffraction peaks are identified shortly after the onset of plastic deformation, proving that a dislocation boundary structure is indeed present during deformation[29]. With further deformation, sharp peaks appear and disappear again (Fig. 4) indicating the transient nature of the dislocation-free regions.

Accompanying the formation of dislocation boundaries, crystal orientation differences arise between adjacent dislocation-depleted regions separated by a boundary. As any misorientation is directly related to an excess of dislocations of one sign (with the misorientation angle inversely proportional to the distance between excess dislocations), misorientations are formed unavoidably from stochastic dislocation storage for all types of boundaries[32]. Based on an ensemble description of dislocations: (i) the evolution of misorientations with plastic strain can be modeled (Fig. 5)[33]; (ii) the universal distribution function for misorientation angles (a Rayleigh distribution) can be derived[34]; (iii) their scaling behavior and deviations at moderate strains explained[35]; and (iv) a constant work-hardening rate at large strains can be predicted[36]; all in accordance with experimental observations[37,38].

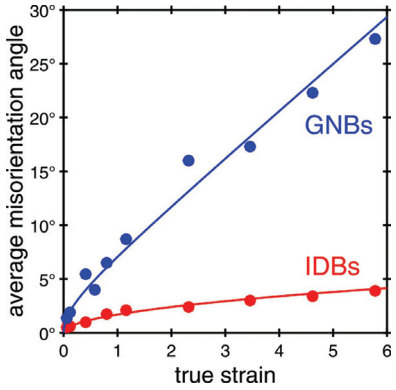

Fig. 5 Evolution of average boundary misorientation angle in cold-rolled Al as a function of plastic strain for different boundary types. Symbols represent experimental data[37,38] and lines indicate model results[36]. For purely statistical accumulation of dislocations in loose boundaries (IDBs), the mean misorientation angle follows a square root law as a function of plastic strain. As a result of differences in slip system activation in the crystallites meeting at a GNB, an additional deterministic contribution to misorientation causes the initial square-root behavior to transition to a linear dependence on plastic strain at larger strains[36].

Dislocation boundary ensembles

As described above, the basic structural elements in deformed metals are dislocation boundaries, each of which is associated with a misorientation angle. The characteristic length in such a structure is the boundary spacing, which decreases with increasing strain while the boundary misorientation angle increases. The morphology of the structures displayed in Fig. 2 remains the same over wide strain ranges.

A universal scaling principle applies to both the spacing[39] and misorientation distributions[37]: the distributions of spacing and misorientation fall on the same curve when normalized with the average value, (Fig. 6). For boundary spacings, this scaling principle is independent of metal type, deformation mode, and strain level[39], applying for average boundary spacings in the range between 10 μm and 10 nm[40]. The fact that the distributions for GNBs and IDBs must be handled separately for scaling purposes[37] further supports the idea that these boundary types have fundamentally different attributes.

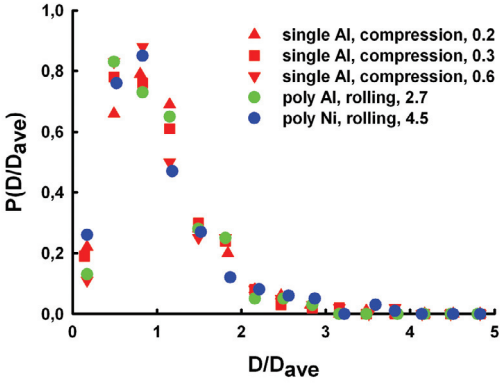

Fig. 6 The distribution of GNB spacing, normalized by the average spacing, scales so that the probability densities collapse to a common curve for a range of metals and deformation conditions. This is exemplified by Al single crystals deformed to three different strains in compression and Al and Ni polycrystals rolled to much higher strains. (Reproduced with permission from[39]. © 2000 Elsevier.)

While adhering to the scaling principle, the local dislocation structure in grains deformed to low strains shows some systematic variations, depending on the grain orientation[41,42]. Structures containing both GNBs and IDBs dominate in the majority of grain orientations. However, some grain orientations only contain IDBs[41]. Fig. 7 shows a stereographic triangle representing all possible grain orientations in tensile deformation[43]. The orientation space is subdivided into three groups with different characteristic structures. Grains with their tensile axes near the crystallographic <100> direction only have IDBs. Grains in the middle of the triangle and near <111> have both GNBs and IDBs. In the middle of the triangle, the GNBs align with crystallographic slip planes, which is not the case for tensile axis orientations near <111>. Apart from the spatial arrangement of the dislocation boundaries, the boundary spacings and misorientation angles also exhibit grain orientation dependence[44]. The grain orientation dependence as a result of the activation of different slip systems in grains of different orientation[45–47].

The accumulation of dislocations during plastic deformation causes metals to harden. This is true whether the dislocations collect in boundaries or are dispersed more or less uniformly throughout grains, as in the case of Al-Mg alloys noted earlier. In general, the flow stress is proportional to the square root of the dislocation density[48,49]. When dislocations are not homogenously distributed but concentrated in boundaries, dislocation emission from boundaries and the interaction of mobile dislocations with boundaries must be the operative hardening mechanisms. This can be analyzed by considering that, for undeformed metals, the flow stress σ depends inversely on the square root of the grain size as given by the Hall-Petch relation[50,51]. For a deformed metal containing dislocation boundaries, replacing the grain size with the GNB spacing allows the flow stress of deformed metals to be modeled[52]. In this case, the proportionality coefficient of the Hall-Petch relation depends on the GNB misorientation angle until a critical angle is reached, after which it becomes constant. Contributions from IDBs are added in the form of dislocation densities, which are calculated based on the IDB spacing and misorientation.

Since GNBs are in general parallel throughout large regions of individual grains, the dependence of flow stress on GNB spacing induces mechanical anisotropy[53–56]. At low strains (1–5%), this can be accounted for by internal stresses[56] but at higher strains, where the GNB structure is well-developed, an additional factor must be involved[55]. At these strains, the flow stress anisotropy has been successfully modeled based on the Hall-Petch relation[57,58], taking into account that the spacing between GNBs encountered by dislocations gliding on different slip planes is different, or based on anisotropic local dislocation densities[59] that reflect the directionality of the GNB structure.

While some general principles for dislocation boundary evolution and the associated mechanical properties have been formulated, many of the underlying mechanisms still remain to be understood. An important example is the decreasing boundary spacing with increasing strain, which is largely accounted for by empirical relations. It has also been demonstrated that the phenomenon cannot be treated in depth without considering individual grains, which exhibit substantially different dislocation structures at low-to-moderate strains. At high strains, the effect of the initial grain orientation becomes less important because of processes at a scale larger than the dislocation boundary spacing.

Mesoscale structure

Within a grain embedded in a polycrystalline aggregate, the amplitude of shear on each slip system may vary as a function of position in the grain. The shear amplitude distribution is reflected in both the localized crystal rotation and the local strain state. The moderate misorientations that develop across GNB boundaries already reflect a moderate shear amplitude difference in the adjoining crystallites; the length scale of the shear amplitude variation within the GNB structure is the boundary spacing. However, in materials with conventional grain sizes, the grain size is 10–1000 times larger than the dislocation boundary spacing. Given the large difference between the dislocation boundary spacing and the spacing of grain boundaries, it is worth considering whether elements of deformation structure can be identified at the mesoscale – a scale in between the GNB spacing and the initial grain size.

Early experimental evidence for grain subdivision at the mesoscale came from slip trace observations[60] showing a patchwork of slip traces on the surface of deformed samples. The slip trace observations

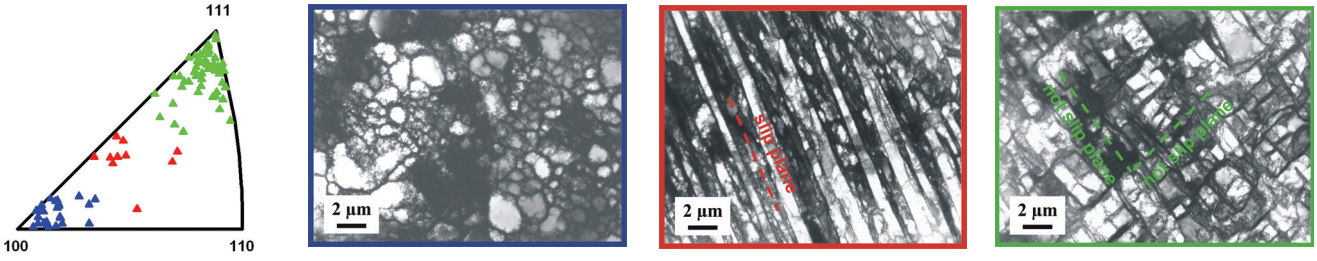

Fig. 7 The stereographic triangle represents all possible crystallographic orientations of the tensile axis. Grains with tensile axes in different parts triangle contain different dislocation structures, as marked with colors. TEM images of these structures are also displayed. Micrographs reproduced from[43].

were quantified by X-ray[61,62], electron diffraction[63–67], and localized strain measurement[68,69] methods, showing that grains embedded in polycrystals often subdivide into orientation domains (often called deformation bands[61]). These are subvolumes of the original grains in which the crystal orientation is roughly constant and differs from that found in other domains originating from the same grain.

The subdivision of grains into mesoscale orientation domains has been detected in a variety of metals and alloys subjected to different macroscopic deformation modes, e.g. tension[67,69], axisymmetric compression[61], plane strain compression[62,66,68], and rolling[64]. In addition to observing the initial stages of grain subdivision, studies of the lamellar microstructures characteristic of rolled, extruded, or drawn materials show that microstructures of the type illustrated in Fig. 2c consist of layers representing different texture components. The distance between high-angle boundaries in the through thickness direction is, on average, several times smaller than the thickness of an initial grain subjected to the geometrical straining process[70]. This shows that several distinct crystal orientations develop from each original grain, indicative of a grain subdivision process.

Experimental evidence that grain subdivision is a common phenomenon at the mesoscale leads to the difficult question: why do grains subdivide into mesoscale domains that represent activation of substantially different slip systems in different regions of an original grain? Requiring individual grains to deform as units, undergoing the same shape change imposed on the polycrystal as a whole, is the assumption at the heart of the well-known Taylor model of polycrystal plasticity[71]. For metals with face-centered cubic (fcc) or body-centered cubic (bcc) crystal structures, orientation subdivision is allowed within the scope of the Taylor model because the high crystal symmetry prompts activation of more slip systems than the minimum number required for each grain to experience the same shape change as the sample as a whole. However, a variety of modeling studies reveal that grain subdivision can also reduce the work of deformation per unit volume compared with the value characteristic of the Taylor model, by reducing the total amplitude of shear distributed across all slip systems. An early grain subdivision model suggested that the central part of a grain could deform in a more arbitrary way, reducing the specific work of deformation in that part of the grain, while the zone of material near the grain periphery mediates incompatibility with neighboring grains[72]. Other models have envisioned grain subdivision into layered structures with compensating shears in neighboring layers[73], an idea similar to groups of self-accommodating martensite plates, which have been widely analyzed by researchers studying thermoelastic martensite transformations[74]. Unfortunately, experimental studies[63–69] and detailed simulation model results[75,76] have failed to reveal compelling evidence of mesoscale domain structures with these characteristic geometries.

A domain structure description in simple metals is gradually emerging from experimental studies; Fig. 8 shows an example. Grains subdivide into blocky domains that exhibit (at most) moderate internal orientation gradients. The IDB and GNB boundaries described earlier are present within each domain. Differences in crystal orientation between domains are accommodated by transition zones (transition bands[62]) in which the orientation changes gradually between the orientations characteristic of the two adjacent domains. Transition zones are initially rather broad (up to roughly one half of the domain dimension) but sharpen as deformation proceeds. As strain increases to values characteristic of industrial rolling processes, the transition zones collapse to single boundaries: the high-angle boundaries between lamellae in rolling microstructures[70].

The factors that influence the geometry and number of domains in one original grain remain incompletely identified. One could envision,

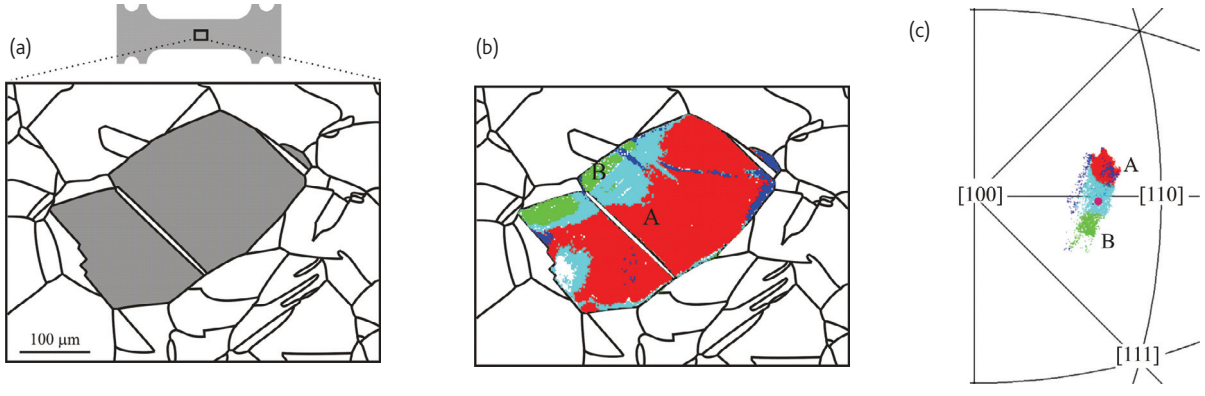

Fig. 8 A grain at the surface of a Cu sample strained 15% in tension. (a) The tensile specimen where the gray shade identifies a grain consisting of three regions separated by thin annealing twins. (b) A map obtained from EBSD measurements. The colors represent domains formed by grain subdivision. (c) A stereographic projection showing the initial tensile axis (pink dot) and the entire range of measured tensile axis orientations after straining (colored cloud). The crystal rotated in one direction throughout the red-colored domain (A), in the opposite direction in the green-colored domain (B), and in a range of intermediate directions in the transition zone (light blue). Dark blue points rotated in directions not consistent with domains A and B or a transition between them. (The rotation analysis is carried out in three dimensions, accounting for the dark blue points with apparently similar orientations as domain A.) The orientation spread within domains A and B is indicative of the misorientations within the structure containing GNBs and IDBs, which are present throughout the grain.

as the ALUMAL model does[77], that domains extend into the center of a grain from grain faces, each domain thus representing a zone of influence of the neighboring grain on the central grain. Such a domain geometry suggests that a domain boundary should emanate from each grain corner (on two-dimensional sections), meeting other domain boundaries near the center of the grain. While domain boundaries can sometimes be found emanating from grain comers, present evidence suggests that this domain geometry is not the most common (Fig. 8, for example).

The comfortable simplicity of the Taylor model, which envisions deformation of grains as units and provides the basis for technologically important global texture predictions[77], is at odds with observations of mesoscale grain subdivision. On the other hand, an industrially useful model based on the prediction of the slip pattern and domain geometry in real microstructures has yet to be developed. Most likely, the factors that influence mesoscale slip patterns will gradually emerge from experimental observations and modeling studies. Blended studies including both experimental and modeling work are likely to contribute much to these advances.

Nanostructured metals by plastic deformation

As described above, gradual refinement of the microstructure occurs during plastic deformation as a result of grain subdivision at several length scales, leading to development of deformation microstructures at the nanoscale if very high strain can be imposed[78,79]. New deformation processes with the potential to achieve strains beyond those attainable by conventional processes have been developed, such as accumulative roll bonding (ARB)[80], equal channel angular extrusion (ECAE)[81], and high-pressure torsion (HPT)[82]. The production of nanostructured metals by these techniques, and the associated significant increase in flow stress because of the structural refinement, has been extensively reported (for a review see elsewhere[83]). The nanostructured metals exhibit characteristic structural features and mechanical behaviors, which are illustrated by the results obtained with ARB-processed commercial purity Al.

Structural parameters

The parameters characterizing nanostructured metals produced by plastic deformation are the same as those used to characterize structures formed at lower strains: domain or grain morphology, boundary spacing, boundary misorientation, and the dislocation density in the volumes between the boundaries. The domain morphology is typically lamellar or equiaxed. Lamellar features are often observed in nanostructures produced by unidirectional deformation, such as cold rolling[84], ARB[85] (Fig. 9a), and HPT[86]. Equiaxed features are typically the result of more complicated deformation modes or strain paths, such as surface mechanical attrition[87], multiple directional forging[88], and ECAE routes involving sample rotation between passes[89]. The domain or grain morphology is also affected by the deformation conditions (e.g. strain, strain rate, and temperature) and material parameters (e.g. stacking fault energy, impurity level, and second phase particles). The boundary spacing in deformation-produced nanostructures is typically in the range of several hundred nanometers to around 100 nm (Fig. 9), while at very large strains the boundary spacing can be reduced to about 10 nm[40,90]. The mean boundary misorientation continuously increases as a function of strain, an extension of the process described in the section on dislocation boundary evolution[91]. Boundary misorientation angles in the deformation-produced nanostructures exhibit a characteristic bimodal distribution with one peak located in the lower end of misorientation angles (e.g. <5°) and the other located in the upper end (e.g. ~50°)[84,92] (Fig. 9b[93]). As a product of high-strain deformation, the deformation-produced nanostructures always contain some dislocations within grains/domains, with the dislocation density depending on the metal and processing conditions.

Mechanical behavior

Tensile properties have been examined for numerous nanostructured metals and alloys[83,94–97] and several common characteristics have been observed: (i) very high strength, several times higher than found for

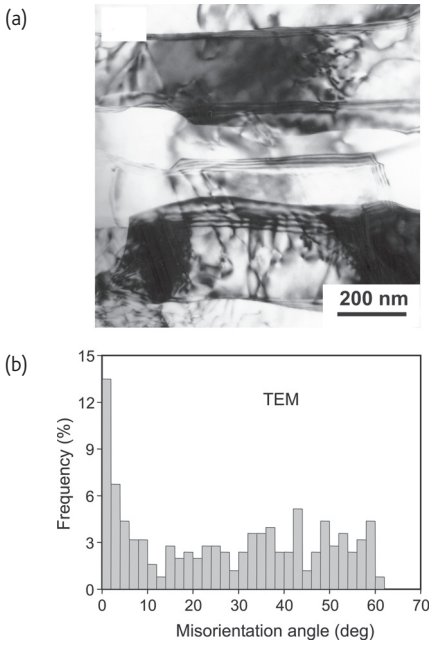

Fig. 9 (a) TEM bright-field image showing a nanometer-scale lamellar structure in commercial purity Al processed by ARB to a strain of 4.8. The presence of individual dislocations (black lines in the volume between the lamellar boundaries) and dislocation tangles are seen. The dislocation density has been measured[85] by an intercept method to be about 1.3 × 10^{14} m^{-2}. (b) Histogram showing the distribution of misorientation angle across the boundaries subdividing the structure[93]. A bimodal misorientation-angle distribution is seen, with one peak located below 3° misorientation and the other located between 40° and 55°. The fraction of high-angle boundaries (>15°) in this structure is 66%.

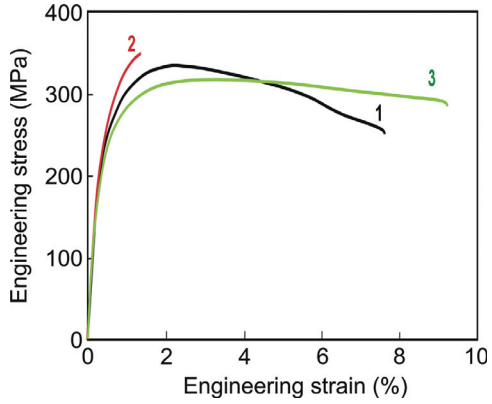

Fig. 10 Tensile stress–strain curves[85] of nanostructured Al processed by ARB to a strain of 4.8. (1) As-ARB processed sample. The yield strength is substantially higher than expected from the Hall-Petch relationship and the tensile elongation is low. (2) ARB + 150°C annealing. Low-temperature annealing causes the material to become stronger and less ductile, contrary to the expectation for metals with conventional grain sizes. (3) ARB + 15% cold rolling. Softening and enhancement of elongation are achieved by slight cold deformation.

coarse-grain samples; (ii) limited strain hardening and small uniform elongation (often less than 3%); and (iii) relatively large post-necking elongation. These features are illustrated in the tensile stress–strain curve of nanostructured Al produced by ARB (curve 1 in Fig. 10)

Because most of the nanostructured metals exhibit limited tensile ductility, optimization of mechanical properties of nanostructured metals and alloys is a key research area and several strategies have been proposed to achieve both high strength and good ductility[98–100]. Structural modification by annealing is one approach. In a recent study[85], we found that after a low-temperature (recovery) annealing treatment, the ARB-processed Al shows an unexpected phenomenon: namely, hardening rather than softening accompanied by a decrease rather than an increase in elongation (curve 2 in Fig. 10). Based on characterization of the structure, it has been proposed that this hardening is caused by enhanced recovery of dislocations during annealing, as a result of interactions between dislocations and closely spaced high-angle boundaries. This structural change leads to a reduction in the density of dislocation sources and, as a consequence, dislocations must be generated from alternative sources, requiring a higher stress for activation during a subsequent deformation interval. This suggestion is supported by an observation of softening when dislocations are reintroduced into the structure by a slight deformation after the annealing treatment. These findings suggest that deformation, rather than annealing, should be explored as a means of improving the ductility of nanostructured metals (curve 3 in Fig. 10)[85].

In summary, nanostructured metals produced by plastic deformation differ quantitatively from recrystallized metals in terms of their characteristic structural parameters. The close spacing of high-angle boundaries in nanostructured metals leads to mechanical properties that are not direct extrapolations of properties found for larger (conventional) grain sizes. Based on these initial findings, further studies of processing techniques may lead to the discovery of additional novel strategies for optimizing the properties of metals with deformation-produced nanostructures.

Outlook

We began by considering techniques used for the study of deformation microstructures in metallic materials. Throughout, we have seen that the development of new techniques plays a central role in expanding our knowledge of deformation microstructures. For example X-ray methods were among the first tools used to probe deformation microstructures, but these methods were largely displaced by TEM when it emerged in the middle of the 20th century. Today, synchrotron X-ray sources enabling the three-dimensional character of microstructural elements to be identified provide novel insight into classic problems in deformation microstructures. The future appears bright for the development and application of even better experimental probes to study deformation microstructures.

Simulation models also have much to contribute. Grain-scale models capable of deformation texture prediction have been intensively developed because of the commercial value of the results. Adapting such models using new insight from experimental results, particularly models to incorporate grain subdivision processes, is ongoing. At a smaller length scale, models based on dislocation/dislocation interactions are on the verge of providing deeper insight into the microscopic processes involved in dislocation boundary formation. Developers of such models will undoubtedly benefit from new experimental techniques that enable smaller volumes of material to be probed, since this information is closer in scale to the model volumes.

In the midst of new developments in both experimental and modeling techniques, one thing has not changed much: the science of deformation microstructures remains largely about images of structures. To a remarkable degree, micrographs remain the medium by which information about deformation microstructures is conveyed. When new experimental techniques produce quantitative information, EBSD measurements for example, our nature seems to compel us to convert those quantitative results into images – 'orientation micrographs' – rather than working with the quantitative information. This is also true for model results. Learning to extract quantitative information from images and finding ways to work directly with the quantitative descriptions is one of the most important challenges in research on deformation microstructures. It is only through progress in this area that we will be able to integrate experimental and modeling studies. mt

Acknowledgments

The authors gratefully acknowledge the Danish National Research Foundation for supporting the Center for Fundamental Research: Metal Structures in Four Dimensions.

REFERENCES

1. Sherby, O. D., and Wadsworth, J., *J. Mater. Processing Technol.*, (2001) **117**, 347
2. Guillet, L., and Portevin, A., *An Introduction to the Study of Metallography and Macrography*, McGraw-Hill, New York, (1922)
3. Williams, D. B. and Carter, C. B., *Transmission Electron Microscopy – A Textbook for Materials Science*, Plenum Press, New York, 1996
4. Novotny, L., and Stranick, S. J., *Annu. Rev. Phys. Chem.* (2006) **57**, 303
5. Baruchel, J., *et al., Scripta Mater.* (2006) **55**, 41
6. Langford, J. I., and Louer, D., *Rep. Prog. in Phys.* (1996) **59**, 131
7. Bunge, H. J., *Texture Analysis in Materials Science, Mathematic Methods*, Butterworths, London, (1983)
8. Kocks, U. F., *et al.*, *Texture and Anisotropy*, Cambridge University Press, Cambridge, (2000)
9. Krieger Lassen, N. C., *et al.*, *Scanning Microscopy* (1992) **6**, 115
10. Humphreys, F. J., *J. Mater. Sci.* (2001) **36**, 3833
11. Juul Jensen, D., *et al.*, *Materials Today* (2006) **9** (1–2), 18
12. Orowan, E., *Z. Phys.* (1934) **89**, 634
13. Polanyi, M., *Z. Phys.* (1934) **89**, 660
14. Taylor, G. I., *Proc. R. Soc. London* (1934) **A145**, 362
15. Sutton, A. P., and Balluffi, R. W., *Interfaces in Crystalline Solids*, Clarendon Press, Oxford, (1995), 139
16. Nabarro, F. R. N., *Theory of Crystal Dislocations*, Clarendon Press, Oxford, (1967)
17. Kröner, E., *Z. Phys.* (1955) **142**, 463
18. Kuhlmann-Wilsdorf, D., *Philos. Mag.* (1999) **79**, 955
19. Kubin, L. P., In *Plastic Deformation and Fracture of Materials*, Mughrabi, H. (ed.), Weinheim, Wiley-VCH, (1992), 137
20. Kuhlmann-Wilsdorf, D., *et al.*, *Scripta Metall. Mater.* (1994) **31**, 729
21. Madec, R., *et al.*, *Scripta Mater.* (2002) **47**, 689
22. Essmann, U., *Phys. Status Solidi* (1965) **12**, 707
23. Steeds, J. W., *Proc. R. Soc. London* (1966) **A292,** 343
24. Bay, B., *et al.*, *Acta Metall. Mater.* (1992) **40,** 205
25. Kuhlmann-Wilsdorf, D., and Hansen, N., *Scripta Metall. Mater.* (1991) **25**, 1557
26. Seeger, A., In *Proc. 8th Int. Conf. Strength of Metals and Alloys* (*ICSMA 8*), Kettunen, P. O., *et al.* (eds.), Pergamon Press, Oxford, (1988), 463
27. Essmann, U., *Phys. Status Solidi* (1963) **3**, 932
28. Mughrabi, H., *Philos. Mag.* (1971) **23**, 869
29. Jakobsen, B., *et al.*, *Science* (2006) **312**, 889
30. Jakobsen, B., *et al.*, *Acta Mater.* (2007) **55**, 3421
31. Jakobsen, B., *et al.*, *Scripta Mater.* (2007) **56**, 769
32. Pantleon, W., *Acta Mater.* (1998) **46**, 451
33. Pantleon, W., *Mater. Sci. Eng. A* (2001) **319**, 211
34. Pantleon, W., *Solid State Phenomena* (2002) **87**, 73
35. Pantleon, W., and Hansen, N., *Acta Mater.* (2001) **49,** 1479
36. Pantleon, W., *Mater. Sci. Eng. A* (2005) **400**, 118
37. Hughes, D. A., *et al.*, *Acta Mater.* (1997) **45**, 105
38. Liu, Q., *et al.*, *Acta Mater.*, (2002) **50**, 3789
39. Godfrey, A., and Hughes, D. A., *Acta Mater.* (2000) **48**, 1897
40. Hughes, D. A., and Hansen, N., *Phys. Rev. Lett.* (2001) **87**, 135503
41. Huang, X., and Hansen, N., *Scripta Mater.*, (1997) **37**, 1
42. Liu, Q., *et al., Acta Mater.* (1998) **46**, 5819
43. Huang, X., *Scripta Mater.* (1998) **38**, 1697
44. Hansen, N., *et al.*, *Mater. Sci. Eng. A* (2001) **317**, 3
45. Winther, G., *Acta Mater.* (2003) **51**, 417
46. Wert, J. A., and Huang, X., *Philos. Mag.* (2003) **83**, 969
47. Shen, K., and Duggan, B., *Acta Mater.* (2007) **55**, 1137
48. Kocks, U. F., *J. Eng. Mater. Technol.* (1976) **98**, 76
49. Kocks, U. F., and Mecking, H., *Prog. Mater. Sci.* (2003) **48**, 171
50. Hall, E., *Proc. Phys. Soc. London B* (1951) **B64**, 747
51. Petch, N., *J. Iron Steel Inst.* (1953) **174**, 25
52. Hansen, N., *Mater. Sci. Eng. A* (2005) **409**, 39
53. Eardley, E. S., *et al.*, *Mater. Sci. Forum* (2003) **426–434**, 363
54. Juul Jensen, D., and Hansen, N., *Acta Metall. Mater.* (1990) **38**, 1369
55. Wilson, D. V., and Bate, P. S., *Acta Mater.* (1996) **44**, 3371
56. Wu, P. D., *et al.*, *Int. J. Plasticity* (2005) **21**, 723
57. Hansen, N., and Juul Jensen, D., *Acta Metall. Mater* (1992) **40**, 3265
58. Li, Z. J., *et al.*, *Acta Mater.* (2006) **54**, 401
59. Peeters, B., *et al.*, *Acta Mater.*, (2001) **49**, 1607
60. Boas, W., and Ogilvie, G. J., *Acta Metall.* (1954) **2**, 655
61. Barrett, C. S., *Trans. AIME* (1939) **135**, 296
62. Dadson, A. B. C., and Doherty, R. D., *Acta Metall. Mater.* (1992) **40,** 345
63. Panchanadeeswaran, S., *et al.*, *Acta Mater.* (1996) **44,** 1233
64. Delannay, L., *et al., Acta Mater.* (2001) **49,** 2441
65. Wu, G. L., *et al.*, *Scripta Mater.* (2001) **45**, 1117
66. Kalidindi, S. R., *et al.*, *Proc. R. Soc. London* (2004) **460**, 1935
67. Thorning, C., *et al.*, *Mater. Sci. Eng. A* (2005) **397**, 215
68. Sachtleber, M., *et al.*, *Mater. Sci. Eng. A* (2002) **336**, 81
69. Tatschl, A., and Kolednik, O., *Mater. Sci. Eng. A* (2003) **339**, 265
70. Hughes, D. A., and Hansen, N., *Acta Mater.* (1997) **45,** 3871
71. Taylor, G. I., *J. Inst. Metals* (1938) **62**, 307
72. Kocks, U. F., and Chandra, H., *Acta Metall. Mater* (1982) **30,** 695
73. Leffers, T., *Int. J. Plasticity* (2001) **17**, 469
74. Saburi, T., *et al.*, *Acta Mater.* (1980) **28,** 15
75. Beaudoin, A. J., *et al., Philos. Mag.* (1996) **73**, 1503
76. Raabe, D., *et al.*, *Acta Mater.* (2002) **50**, 421
77. Van Houtte, P., *et al.*, *Int. J. Plasticity* (2005) **21**, 589
78. Valiev, R. Z., *et al.*, *Prog. Mater. Sci.* (2000) **45**, 103
79. Zhu, Y. T., and Langdon, T. G., *J. Metals* (2004) **56** (10), 58
80. Tsuji, N., *et al.*, *Adv. Eng. Mater.* (2003) **5**, 338
81. Segal. V. M., *Mater. Sci. Eng. A* (1995) **197**, 157
82. Valiev, R. Z., *Mater. Sci. Eng. A* (1997) **234,** 59
83. Meyers, M. A., *et al., Prog. Mater. Sci.* (2006) 51, 427
84. Hughes, D. A., and Hansen, N., *Acta Mater.* (2000) **48**, 2985
85. Huang, X., *et al.*, *Science* (2006) **312**, 249
86. Huang, X., *et al.*, In *Ultrafine Grained Materials III*, Zhu, Y. T., *et al.*, (eds.), The Minerals, Metals, and Materials Society, Warrendale, (2004), 235
87. Zhang, H. W., *et al.*, *Acta Mater.* (2003) **51**, 1871
88. Sitdikov, O., *et al.*, *Philos. Mag.* (2005) **85**, 1159
89. Furukawa, M., *et al.*, *Mater. Sci. Eng. A* (2002) **332**, 97
90. Zhang, H. W., and Hansen, N., *J. Mater. Sci.* (2007) **42**, 1682
91. Hansen, N., *Metall. Mater. Trans. A* (2001) **32**, 2917
92. Liu, Q., *et al., Acta Mater.* (2002) **50**, 3789
93. Huang, X., *et al., Mater. Sci. Eng. A* (2007) doi:10.1016/j.msea.2006.10.173
94. Hansen, N., *Scripta Mater.* (2004) **51**, 801
95. Wang, Y. M., and Ma, E., *Acta Mater.*, (2004) **52**,1699
96. Koch, C. C., *et al., Adv. Eng. Mater.* (2005) **7**, 787
97. Sanders, P. G., *et al., Mater. Sci. Eng. A* (1997) **234**, 77
98. Wang, Y. M., *et al., Nature,* (2002) **419**, 912
99. Zhao, Y. H., *et al., Adv. Mater.* (2006) **18**, 2280
100. Lu, L., *et al., Science* (2004) **304**, 422